NASA CASE NO. NPO-18702-1-CU

PRINT FIG. 10

NOTICE

The invention disclosed in this document resulted from research in aeronautical and space activities performed under programs of the National Aeronautics and Space Administration. The invention is owned by NASA and is, therefore, available for licensing in accordance with the NASA Patent Licensing Regulation (14 Code of Federal Regulations 1245.2).

To encourage commercial utilization of NASA-Owned inventions, it is NASA policy to grant licenses to commercial concerns. Although NASA encourages nonexclusive licensing to promote competition and achieve the widest possible utilization, NASA will consider the granting of a limited exclusive license, pursuant to the NASA Patent Licensing Regulations, when such a license will provide the necessary incentive to the licensee to achieve early practical application of the invention.

Address inquiries and all applications for license for this invention to NASA Patent Counsel, NASA Resident Office-JPL, Mail Code 180-801, 4800 Oak Grove Drive, Pasadena, CA 91109.

Approved NASA forms for application for nonexclusive or exclusive license are available from the above address.

Serial Number: 07/842,300

Filed Date: February 26, 1992

NRO-JPL

JPL Case No. 18702
NASA Case No. NPO-18702-1-CU
Attorney Docket No. JPL-25

PATENT APPLICATION

ELECTRO-OPTIC RESONANT PHASE MODULATOR

ORIGIN OF INVENTION

The invention described herein was made in the performance of work under a NASA contract, and is subject to the provisions of Public Law 96-517 (35 USC 202) in which the Contractor has elected not to retain title.

TECHNICAL FIELD

The present invention relates generally to coherent optical communications and more specifically to coherent phase modulated optical communications wherein a high data rate resonant phase modulator operates with low driving voltages.

BACKGROUND ART

Coherent optical communication technology can provide improved receiver sensitivity compared to direct detection systems in many applications. By amplifying the weak incident signal with a strong local oscillator (LO) output, the system can overcome thermal noise limitations and achieve near quantum-limited sensitivity. In addition, coherent reception offers a better background noise rejection capability since the spectral filtering is performed at the intermediate frequency where the bandwidth can be much more selective. The bandwidth selective nature of the coherent receiver can also lead to a more efficient use of the optical spectrum and the potential of multiple-access communications over a single lasing bandwidth.

In order to realize the full benefits of the coherent system, it is desirable that the transmitted optical signal be phase encoded. Phase encoding provides optimal energy efficiency, and is particularly desirable for deep-space missions where the signal power is at a premium. At the receiving end, the optical signal is coherently detected by spatially

mixing the incoming signal with a local oscillator laser output and then detecting it using a balanced detector receiver. Phase modulation of semiconductor lasers can be accomplished by modulating the injection current density and hence the instantaneous frequency of the laser. For CW lasers such as diode pumped solid state lasers an external modulator will be required. Bulk electro-optical (EO) phase modulation often requires high modulation voltage that is not practical to achieve in a flight system. Several approaches can be used to lower the driving voltage requirement. The techniques include travelling wave modulators with long interaction lengths and waveguide modulators with narrow channels (C.M. Gee, G.D. Thurmond and H.W. Yen, "Travelling-Wave Electro-Optic Modulator", Appl. Opt., Vol. 22, No. 13, pp. 2034-2037, July, 1983; I.P. Kaminow, J.R. Carruthers, E.H. Turner, and L.W. Stulz, "Thin-Film $LiNbO_3$ Electro-Optic Light Modulator", Appl. Phys. Lett., Vol. 22, No. 10, pp. 540-542, May, 1973). Resonant modulators in which the optical and RF modulation signals are both resonated to improve the modulation efficiency have also been proposed and implemented (T.F. Gallagher, N.H. Tran and J.P. Watjen, "Principles of Resonant Cavity Optical Modulator", Appl. Opt., Vol. 25, No. 4, pp. 510-514, Feb. 1986;

W.J. Stewart, I. Bennion and M.J. Goodwin, "Electro-Optic Resonant Waveguide Modulation", Tenth European Conference On Optical Communication, Sept. 1984). In order to match the group velocity of optical and RF signals, however, these devices tend to have a narrow modulation bandwidth and cannot be extended to broadband operation needed for data modulation. An alternative is to use only a resonant optical cavity which enhances the interaction length without complex electrode configuration to match the optical and electronic group velocity (W.J. Stewart, I. Bennion and M.J. Goodwin, "Resonant Modulation", Phil. Trans. R. Soc. Lond. A313, p. 401, 1984). Since no electrical resonator is used, the method can in principle be operated at near demodulation frequency. The upper limit of modulation bandwidth is limited by the finesse and hence the cavity lifetime. A resonant ring cavity using this principle has been under investigation for coherent communication (T.J. Kane and R.W. Wallace, "Coherent Communication Link Using Diode-Pumped Lasers", Final Report for Contract NAS5-30487 for NASA Goddard Space Flight Center, August 1989). The present invention relates to an electro-optic resonant phase modulator which as been designed to operate at 100 Mbps. Previously, resonant cavities have also been explored fo amplitude modulation (F.R. Nash and P.W. Smith, "Broadband Optical Coupling Modulation",

IEEE J. Quantum Electron, Vol. QE-4, pp. 26-34, 1968; D.M. Henderson an V.A. Vilnrotter, "Optical Coupling Modulation In Travelling-Wave Cavities", Appl. Phys. Lett., Vol. 30, No. 7, pp. 335-337, April 1977). The concept of resonant cavity has also been extended to temperature sensors and high-speed signal processing (R.R.A. Syms, "Resonant Cavity Sensor for Integrated Optics", IEEE Journal of Quantum Electronics, Vol. QE-21, No. 4, April, 1985) and a passive resonant ring cavity laser gyroscope has been investigated as an alternative to the standard Sagnac interferometer laser gyroscope (K.A. Pugh, "Design, Construction, and Analysis of An Ultra-Low Expansion Quartz Resonant Cavity Passive Ring Resonator Laser Gyroscope", Master of Science Thesis, Air Force Institute of Technology Air University, March 1982).

STATEMENT OF THE INVENTION

A resonant cavity electro-optic phase modulator has been designed and implemented to operate at a data rate of 100 Mbps. The modulator consists of an electro-optic crystal located in a highly resonant cavity. The cavity is electro-optically tuned on and off resonance, and the phase dispersion near the cavity resonance provides the output phase modulation. The performance of the modulator was measured by first heterodyne detecting the signal to an intermediate frequency and then measuring the spectral characteristics using an RF spectrum analyzer. The measured phase shift is shown to be in good agreement with the theoretical predictions.

OBJECTS OF THE INVENTION

It is therefore a principal object of the present invention to provide an electro-optic resonant phase modulator wherein phase modulation is achieved with reduced driving voltages.

It is an additional object of the invention to provide an electro-optic resonant phase modulator wherein a phase modulation data rate of 100 Mbps is provided with switching voltages less than 10 Volts.

It is still an additional object of the invention to provide an external cavity phase modulator for electro-optics communication and employing a voltage switched electro-optic crystal for detuning the cavity from resonance at a high data rate using relatively low voltage.

BRIEF DESCRIPTION OF THE DRAWINGS

The aforementioned objects and advantages of the present invention, as well as additional objects and advantages thereof, will be more fully understood hereinafter as a result of a detailed description of a preferred embodiment when taken in conjunction with the following drawings in which:

FIG. 1 is a conceptual illustration of a Gire-Turnois etalon which is a prior art realization of a resonant cavity;

FIG. 2 is a graph of output phase dispersion and intensity variation versus the cavity detuning for a cavity with 85% input coupler reflectivity;

FIG. 3 is a generalized illustration of a phase modulator according to the present invention;

FIG. 4 is a graph of output phase versus applied modulation voltage for cavities with different values of input coupler reflectivity;

FIG. 5 is a graph of output intensity versus intracavity loss for a resonant cavity modulator with different values of input coupler reflectivity;

FIG. 6 is a graph of output phase shift versus time for a resonant cavity with different values of input coupler reflectivity;

FIG. 7 is a graph of required switching time for the output phase to shift from $-\pi/2$ to $+\pi/2$ for a resonant cavity phase modulator with different values of input coupler reflectivity;

FIG. 8, comprising FIGs. 8(a), 8(b), 8(c) and 8(d), is a graphical illustration of the periodic modulation signal of FIG. 8(a), wherein FIG. 8(b) shows the resulting output intensity for a cavity biased on resonance and FIGs. 8(c) and 8(d) illustrate output intensity when the cavity is biased off resonance;

FIG. 9 is a display image of a typical error curve for the resonant cavity modulator driven by a pseudo-random data sequence wherein the horizontal axis represents the cavity detuning;

FIG. 10 is a block diagram of an experimental configuration of the present invention; and

FIG. 11, comprising FIGs. 11(a), 11(b) and 11(c) is the observed IF spectrum of the resonant cavity phase modulator when driven by a 0.2 Volt sinusoid, a 5.5 Volt sinusoid and a 10 Volt amplitude pseudo-random data sequence.

DETAILED DESCRIPTION OF A PREFERRED EMBODIMENT

The phase modulator of the invention is an external cavity phase modulator in which an optical cavity is biased near resonance to the incident laser beam. Since the phase angle of the reflected signal from a tuned cavity is highly dispersive near the resonance, a small detuning of the cavity from resonance can result in a large output phase shift. By modulating the cavity near its resonance, therefore, the output phase can be modulated.

A particular realization of the resonant cavity is the Gire-Turnois etalon shown in FIG. 1. The etalon consists of a partially reflective input coupler with reflectivity R and a highly reflective back mirror. The incoming signal E_i , the reflected signal, E_o satisfy the following relationship:

$$\begin{pmatrix} E_t \\ E_r \end{pmatrix} = \begin{pmatrix} t & r \\ -r^* & t^* \end{pmatrix} \cdot \begin{pmatrix} E_i \\ E_t \end{pmatrix} , \qquad (1)$$

where $|t|^2 = T$ and $|r|^2 = R$ are the transmittance and reflectivity of the input coupler, and E_t , E_r are the transmitted amplitude into the etalon, and the

reflected signal from the back surface, respectively. T + R = 1 by conservation of energy. Without loss of generality, both r and t can be chosen as real numbers. A round trip within the cavity will pick up an equivalent phase shift ϕ and an amplitude gain g such that

$$E_r = ge^{i\phi} \cdot E_t \quad . \tag{2}$$

Equations (1) and (2) can be solved for the relationship between input and output fields. The result is

$$E_o = \left[\frac{ge^{i\phi} - r^*}{1 - rge^{i\phi}}\right] E_i \quad . \tag{3}$$

The output intensity and phase shift, Φ , can be solved from Equation (3) as

$$I_o/I_i = \frac{G + R - 2\sqrt{GR}\cos\phi}{1 + GR - 2\sqrt{GR}\cos\phi} \quad . \tag{4}$$

$$\Phi = \tan^{-1}\left[\frac{\sqrt{G}(1-R)\sin\phi}{-\sqrt{R}(1+G) + \sqrt{G}(1+R)\cos\phi}\right] \quad , \tag{5}$$

where $G = |g|^2$ is the effective gain of the cavity. $G \leq 1$ for a passive cavity shown in FIG. 1

Shown in FIG. 2 is a plot of the reflected intensity and phase versus the cavity detuning ϕ. When $\phi = 0$, the cavity is in resonance with the incoming signal. In this case the reflected signals is in phase with the incoming signal. When the cavity is slightly off resonance, however, the reflected signal experiences a phase shift which is highly dispersive near the cavity resonance. The reflected intensity also experiences variation as the cavity is tuned across resonance. Since the back mirror of the cavity has high reflectivity, most of the energy is reflected into the incident direction. When the cavity is off resonance, the reflected intensity is very close to the incident intensity. When the cavity is tuned near resonance, on the other hand, small absorption/scattering loss within the cavity can multiply as the number of passes through the cavity increases and result in a drop in the output intensity. This absorption dip is generally undesirable since it reduces the amount of output signal power. However, it can also be used to provide the error signal for locking the cavity near resonance with the incoming laser.

The large phase dispersion experienced by the Gire-Turnois etalon as it is tuned across its resonance can be used to modulate the phase of the reflected optical signal from the cavity if the effective cavity length can be modulated by an externally applied electrical signal. The resulting phase modulator is shown in FIG. 3 in which an electro-optic (EO) crystal is situated between the front and back surface of the etalon. The index of refraction and hence the optical path length through the EO crystal can be modulated by applying a voltage signal. The cavity is normally biased near its reflective resonance with the incoming laser light. A small voltage signal across the EO crystal will therefore result in a detuning angle ϕ which can be related to the applied voltage V and the half wave voltage V_π of the EO crystal by

$$\phi = 2\pi V/V_\pi \quad . \tag{6}$$

The factor of two in Equation (6) is introduced since the optical signal traverses twice through the crystal per round trip for a linear cavity. The half wave voltage for a 3m crystal cut for phase modulation is given by

$$V_\pi = \frac{\lambda}{n^3 r_{33}} \frac{d}{\ell} \quad , \tag{7}$$

where λ is the wavelength, n is the index of refraction, r_{33} is the electro-optic coefficient, d is the thickness of the crystal, and ℓ is the length of the crystal.

The steady-state phase shift performance of the modulator can be easily evaluated using Equation (5) and the results are plotted in FIG. 4 as a function of the input voltage for different values of mirror reflectivity. The plot is generated assuming zero intracavity loss (G = 1). It is seen that the output phase shift per unit voltage input increases as the reflectivity increases. For a highly tuned cavity, only a small voltage needs to be applied to produce a large output phase shift. On the other hand, it can be seen from FIG. 4 that cavity with high reflectance input coupler is very sensitive to intracavity losses.

The dependence of the output intensity versus the intracavity loss ρ = 1- G is plotted in FIG. 5. It is seen that the output intensity is very sensitive to the intracavity loss when the cavity finesse is high. This is because for a high finesse cavity the optical signal traverses through the cavity many times. Consequently any loss within the cavity can result in a significant

loss at the output. As the input coupler reflectivity and hence the finesse of the cavity decrease, the output intensity becomes less sensitive to the intracavity loss.

Transcient response to step switching voltage, on the other hand, cannot be predicted using Equation (5). Time domain response is in general a complicated function of the cavity finesse, the intracavity loss, and the cavity length; and cannot be expressed in a closed-form. In order to calculate the build-up of the resultant phase shift as a function of intracavity loss, output mirror reflectivity, applied voltage and time, a computer model of the phase modulator was developed to simulate the response. The phase shift after successive round trips in the modulator can be modeled as

$$\begin{aligned} E_t(N) &= tE_i + rgE_t(N-1)e^{i\phi(t)} \\ E_o(N) &= -rE_i + tgE_t(N-1)e^{i\phi(t)} \end{aligned} \quad , \tag{8}$$

where $E_t(N)$ and $E_o(N)$ are the amplitudes of the circulating and the output fields after the N^{th} round trip, respectively. Both amplitude transmittance and reflectance have been modeled as real numbers. Any

phase shift can be absorbed into the round trip phase shift, ϕ . After each round trip, the circulating field experiences a net phase shift of ϕ . After a sufficient number of iterations, the output phase shift converges to a value given by Equation (5). The resultant phase shift build-up, based on the simulations, is graphed in FIG. 6 as a function of time for different coupler reflectivities. In this simulation, the applied voltage has been modeled as a step function. As seen from FIG. 6, cavities with lower reflectivity mirrors have faster switching times. Shown in FIG. 7 is a plot of the switching time versus cavity length for several input coupler reflectivities. Again, it is seen that cavities with lower finesse have faster switching times.

In order to achieve a reasonable performance at 100 Mbps, it is desirable that the pulse rise time be shorter than 4 ns. Furthermore, since the complexity of constructing a high voltage driver increases rapidly with voltage requirements, it is desirable to limit the maximum amount of voltage applied to the modulator to less than 20V. From previous analysis, it is known that there are design trade-offs between rise time and cavity finesse, and between required switching voltage

and cavity finesse. A low finesse cavity generally has a faster switching time, but requires higher switching voltage. On the other hand, cavity finesse cannot be increased indefinitely as the switching time also increases with cavity finesse. Furthermore, there is a tradeoff between the half-wave voltage of the EO crystal with its aspect ratio, i.e., thin crystal has a lower half wave voltage, but is more difficult to align. Several point designs for the modulator using different values of input coupler reflectivity were evaluated. Shown in Table 1 are the resulting designs that satisfy the above stated performance requirements.

TABLE 1

Input Coupler Reflectivity	Crystal/Cavity Length (mm)	Crystal Thickness (mm)	Switching Time (ns)	Voltage (V)	Max Intracavity Loss for 80% Thruput (%)
90%	5.0 / 7.0	1.0	3.1	10	0.5
85%	10.0 / 12.0	1.0	3.4	10	0.9
80%	15.0 / 17.0	1.5	3.7	11	1.2
70%	25.0 / 27.0	2.0	3.8	14	2.0

Among them, the 90% reflectance design requires an intracavity loss less than 0.5% which is difficult to achieve. Cavity design using reflectivities less than 80% require EO crystals with high aspect ratio. These designs are undesirable since they are difficult to align. The 85% reflectance design was selected based on the ease of alignment, short rise time, and its tolerance to intracavity losses.

From FIG. 2, it is seen that the strong phase dispersion occurs only when the cavity is biased on resonance. A cavity biased away from resonance will have little or no response to the modulation voltage. Consequently, in order for the external cavity to exhibit a strong phase modulation characteristics, the cavity must be maintained on resonance with the incoming laser signal.

Cavity stabilization can be accomplished using a variety of different means. For the 100 Mbps modulator, cavity stabilization is achieved by monitoring the drop off of output intensity due to absorption of signal near resonance. The principle is illustrated in FIG. 8 where the output intensity is plotted against the cavity detuning for cavities biased

on resonance and at either side of the resonance. Shown in the left-hand side of FIGs. 8(b)-(d) is the output intensity versus cavity detuning, which is being modulated by a periodic sequence shown in FIG. 8(a). When the cavity is biased on resonance, the symmetric displacement at both sides of the absorption dip result in an output intensity modulation that is at twice the frequency of the modulation signal. When the cavity is biased away from resonance, however, the modulation result in asymmetric displacement around the absorption dip. In this case the output intensity exhibits a frequency component at the modulation frequency. Depending on the direction of cavity detuning, this intensity fluctuation signal can be either in-phase or 180 degrees out of phase with the modulation voltage. By correlating the output intensity with the driving signal, therefore, an error voltage can be derived for maintaining the cavity on resonance. Shown in FIG. 9 is the error signal as the cavity is swept across its resonance. Notice the strong locking signal near the cavity resonance.

Although the locking technique was described using a periodic modulation signal, it is straightforward to show that the correlation characteristics and hence the error signal remains identical for nonperiodic input signals. As a result, the random data stream for the communication channel can be used to provide the necessary dither to the cavity and hence maintain the cavity on resonance with the incoming laser signal. In practice, instead of monitoring the output intensity directly, the cavity can be stabilized by sensing the small leakage of signal from the backside of the high reflectance mirror.

Shown in FIG. 10 is a block diagram of a tested configuration. The resonant cavity consists of a 1 cm-long EO crystal and a high reflectance (HR) back mirror. One side of the EO crystal is coated with a 85% reflective coating, and used as the input coupler to the resonant cavity. The second side of the EO crystal is anti-reflection coated to reduce intracavity loss. The HR back mirror has a 20 cm radius of curvature. The long radius of curvature is chosen to reduce the sensitivity to mode matching optics. A 2 mm air gap between the EO crystal and the back mirror results in an effective cavity length of 12 mm.

A 10 cm focal length lens is used to mode match the output signal from a Lightwave Model 120-01A laser into the modulation cavity. Since the input and output beams are collinear, a two-stage Faraday isolator is used to separate the two beams.

A focusing lens and a photodetector positioned at the back of the HR mirror senses the small leakage signal for cavity stabilization purposes. This signal is subsequently amplified and mixed with a properly delayed version of the modulation data stream using an RF mixer. The delay between two arms is adjusted such that the same error curve shown in FIG. 9 is obtained at different modulation frequencies. The output of the mixer is then filtered using a low pass integrator and the output of the integrator is fed into a high voltage amplifier to bias the EO crystal.

The phase shifted output is examined using an optical heterodyne receiver. The amplitude of the detected IF signal is proportional to that of the input optical signal. The amount of phase shift as a function of the input voltage can be measured by applying a sinusoidal modulation voltage and observing the resulting IF spectrum. If the phase modulator responds linearly

with modulation voltage, the resulting phase modulated IF signal can be decomposed into a sum of pure sinusoids at difference harmonics as

$$\sin(\omega t + \Phi \sin \omega_m t) = \sum_{n=0}^{\infty} J_n(\Phi) \sin(\omega + n\omega_m)t + \sum_{n=1}^{\infty} J_n(\Phi) \sin(\omega - n\omega_m)t \quad , \tag{9}$$

where ω and ω_m are the IF carrier and modulation frequencies, respectively, $J_n(\Phi)$ is the n^{th} order Bessel function, and Φ is the modulation index of the phase modulated signal. From Equation (9), it is seen that the amount of IF signal power falls within the k^{th} sideband is proportional to $J_n^2(\Phi)$. Experimentally, the phase modulation index can be determined by measuring the sideband powers, then adjusting the parameter Φ until an optimal fit was obtained between the predicted sideband powers and the experimentally measured results. One method of fitting the data is to minimize the mean square error given by

$$E_D(\Phi) = \sum_{n=1}^{k} \left[10 \log \left(\frac{J_n(\Phi)}{J_0(\Phi)} \right)^2 - (P_n - P_0) \right] \quad , \tag{10}$$

where we have denoted the measured power within the n^{th} sideband by P_n. The measured sideband powers are normalized with respect to the carrier power. This allows us to deduce the phase shift without an absolute power measurement.

In principle, the method outlined in Equations (9) and (10) is more accurate when more sidebands are measured. Unfortunately, this is true only when the modulator has a linear response and infinite bandwidth. The resonant cavity phase modulator, however, has an inherent bandwidth constraint. Furthermore, the intracavity loss introduces an amplitude modulation that also modifies the IF spectrum. Equation (10) must therefore be properly modified in order to estimate the amount of phase shift for the resonant cavity modulator. This is accomplished using the computer simulation model given in Equation (8). The simulated response of the phase modulator with respect to sinusoidal modulation voltage is Fourier transformed to generate the predicted sideband powers. These sideband powers are then correlated with the measured sideband powers to derive the estimated phase shift performance. Shown in FIGs. 11(a) and 11(b) are the resulting IF spectrum for phase modulation of 0.2 rad and 1.6 rad, respectively. Note that the carrier power is suppressed at large modulation index as expected. Also shown in FIG. 11(c) is the IF spectrum when the modulator is driven by a 23 bit pseudo random data sequence at modulation voltage of 10 V. Note the near complete suppression of the IF carrier as expected.

It will now be understood that what has been disclosed herein comprises an external resonant cavity phase modulator for coherent electro-optic devices such as CW lasers. Phase modulation of a laser output beam at extremely high data rates (i.e., 100 Mbps) and with relatively low voltage (i.e., 10 Volts) is demonstrated. A feedback system is used to correlate the modulated light and the modulating voltage to lock the cavity to the resonance of the laser output by appropriately biasing the electro-optic crystal of the modulator.

Having thus described an exemplary embodiment of the invention, what is claimed is:

JPL Case No. 18702 PATENT APPLICATION
NASA Case No. NPO-18702-1-CU
Attorney Docket No. JPL-25

~~31~~ 26

ELECTRO-OPTIC RESONANT PHASE MODULATOR

ABSTRACT OF THE DISCLOSURE

An electro-optic resonant cavity is used to achieve phase modulation with lower driving voltages. Laser damage thresholds are inherently higher than with previously used integrated optics due to the utilization of bulk optics. Phase modulation is achieved at higher speeds with lower driving voltages than previously obtained with non-resonant electro-optic phase modulators. The instant scheme uses a data locking dither approach as opposed to the conventional sinusoidal locking schemes. In accordance with a disclosed embodiment, a resonant cavity modulator has been designed to operate at a data rate in excess of 100 Mbps. By carefully choosing the cavity finesse and its dimension, it is possible to control the pulse switching time to within 4 ns and to limit the required switching voltage to within 10 V. Experimentally, the

resonant cavity can be maintained on resonance with respect to the input laser signal by monitoring the fluctuation of output intensity as the cavity is switched. This cavity locking scheme can be applied by using only the random data sequence, and without the need of additional dithering of the cavity. Compared to waveguide modulators, the resonant cavity has a comparable modulating voltage requirement. Because of its bulk geometry, resonant cavity modulator has the potential of accommodating higher throughput power. Furthermore, mode matching into a bulk device is easier and typically can be achieved with higher efficiency. On the other hand, unlike waveguide modulators which are essentially traveling wave devices, the resonant cavity modulator requires that the cavity be maintained in resonance with respect to the incoming laser signal. An additional control loop is incorporated into the modulator to maintain the cavity on resonance.

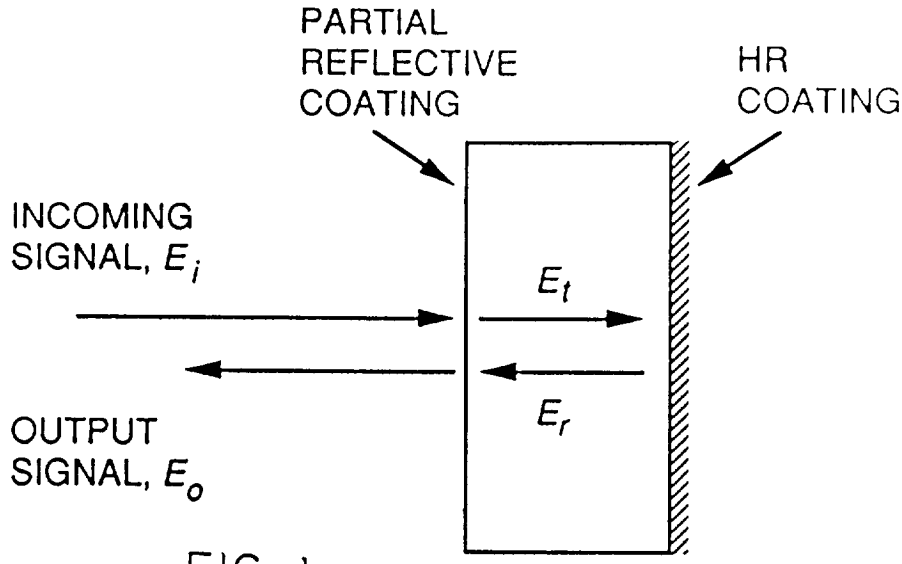
PARTIAL
REFLECTIVE
COATING
HR
COATING
INCOMING
SIGNAL, E_i
E_t
E_r
OUTPUT
SIGNAL, E_o

FIG. 1

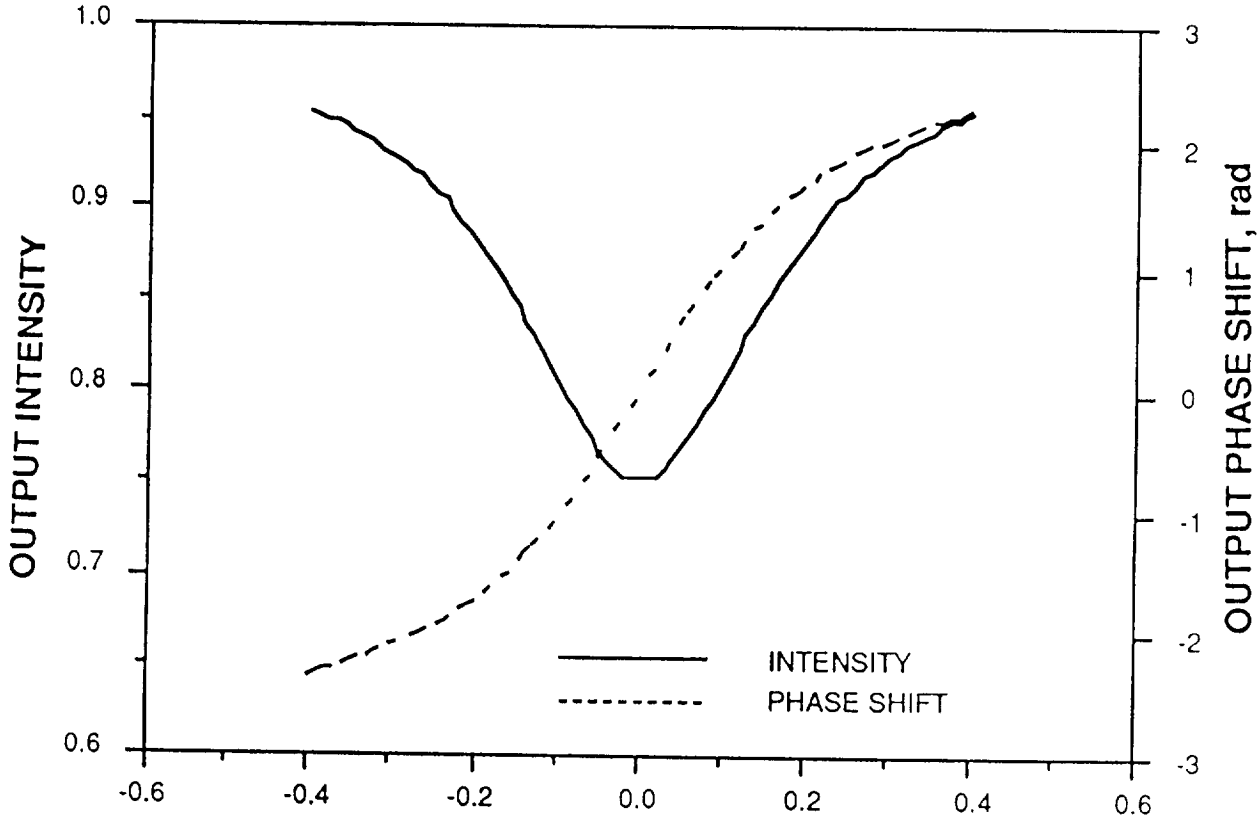
1.0
0.9
0.8
0.7
0.6
OUTPUT INTENSITY
3
2
1
0
-1
-2
-3
OUTPUT PHASE SHIFT, rad
INTENSITY
PHASE SHIFT
-0.6
-0.4
-0.2
0.0
0.2
0.4
0.6
CAVITY DETUNING, rad

FIG. 2

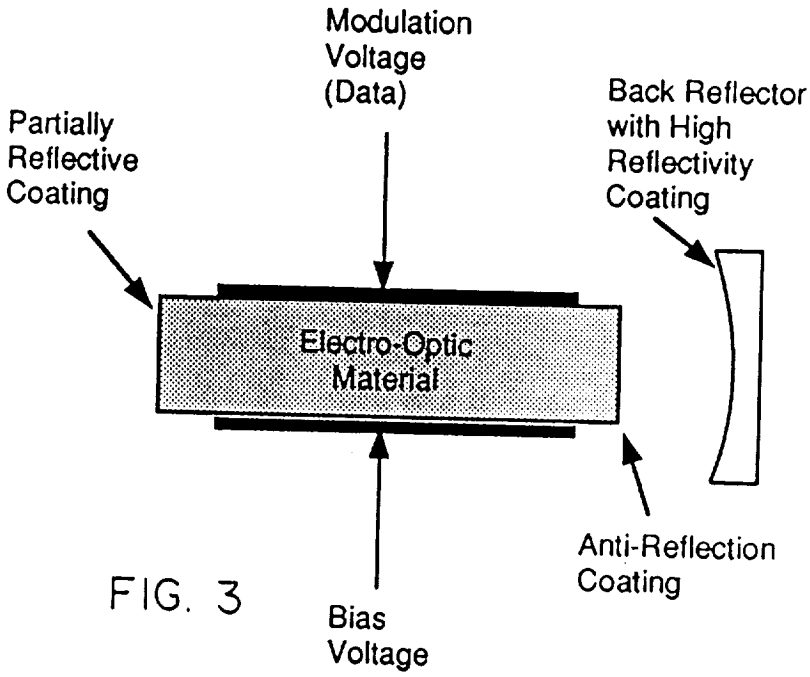
Modulation
Voltage
(Data)
Partially
Reflective
Coating
Back Reflector
with High
Reflectivity
Coating
Electro-Optic
Material
Anti-Reflection
Coating
Bias
Voltage

FIG. 3

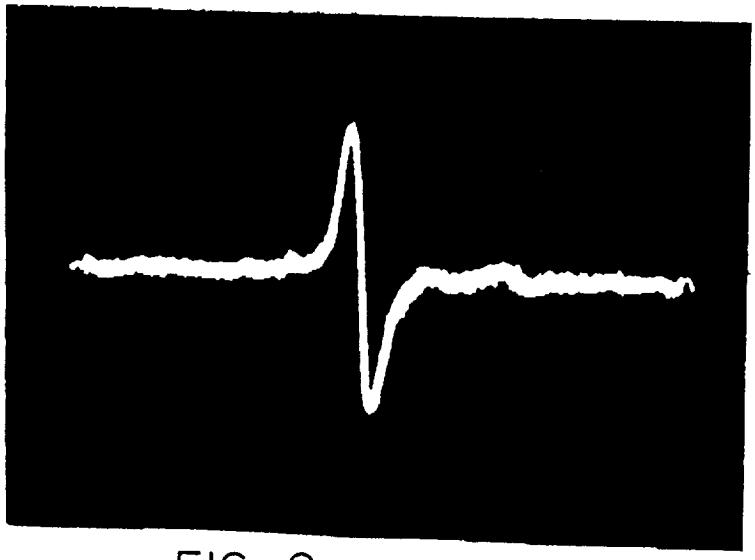

FIG. 9

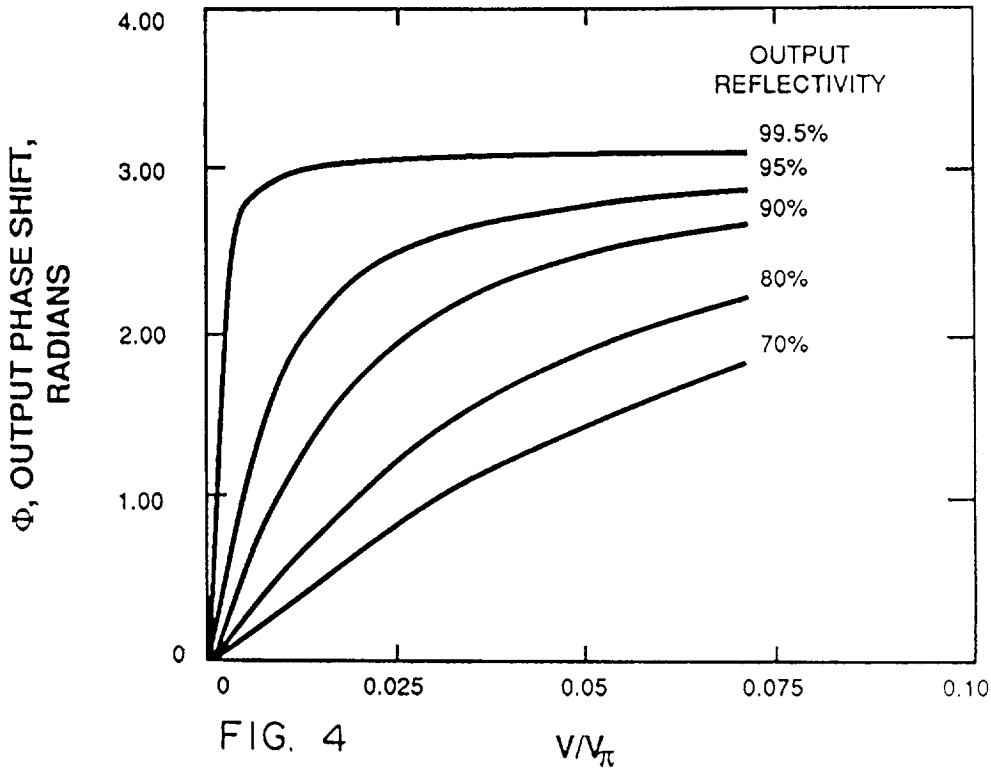
4.00
3.00
2.00
1.00
0
Φ, OUTPUT PHASE SHIFT, RADIANS
OUTPUT REFLECTIVITY
99.5%
95%
90%
80%
70%
0
0.025
0.05
0.075
0.10
V/Vπ

FIG. 4

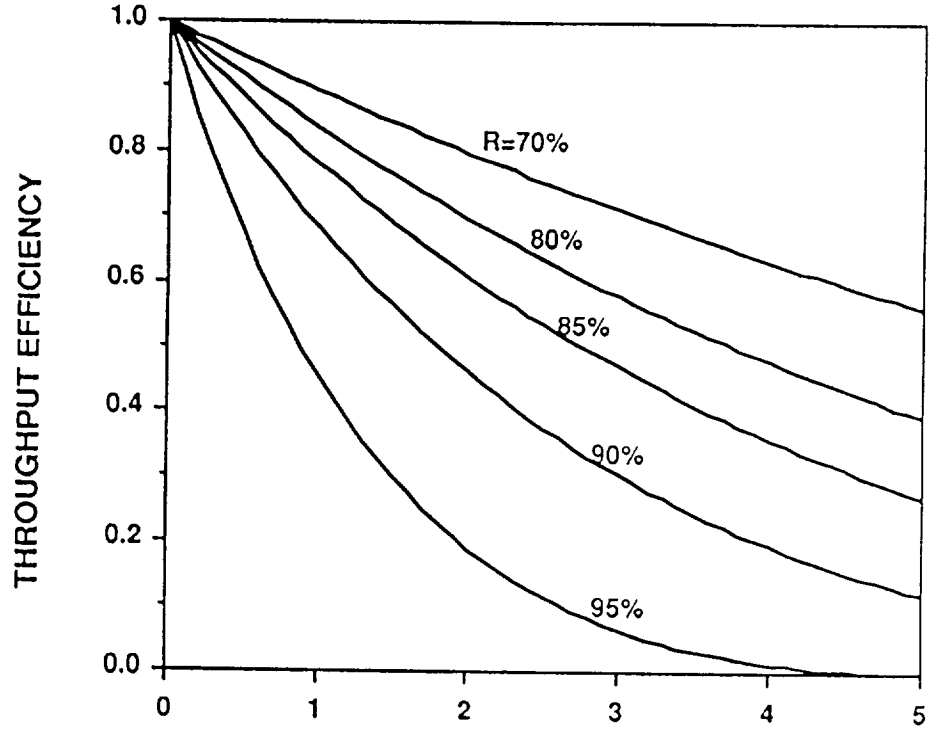
1.0
0.8
0.6
0.4
0.2
0.0
THROUGHPUT EFFICIENCY
R=70%
80%
85%
90%
95%
0
1
2
3
4
5
INTRACAVITY LOSS, %

FIG. 5

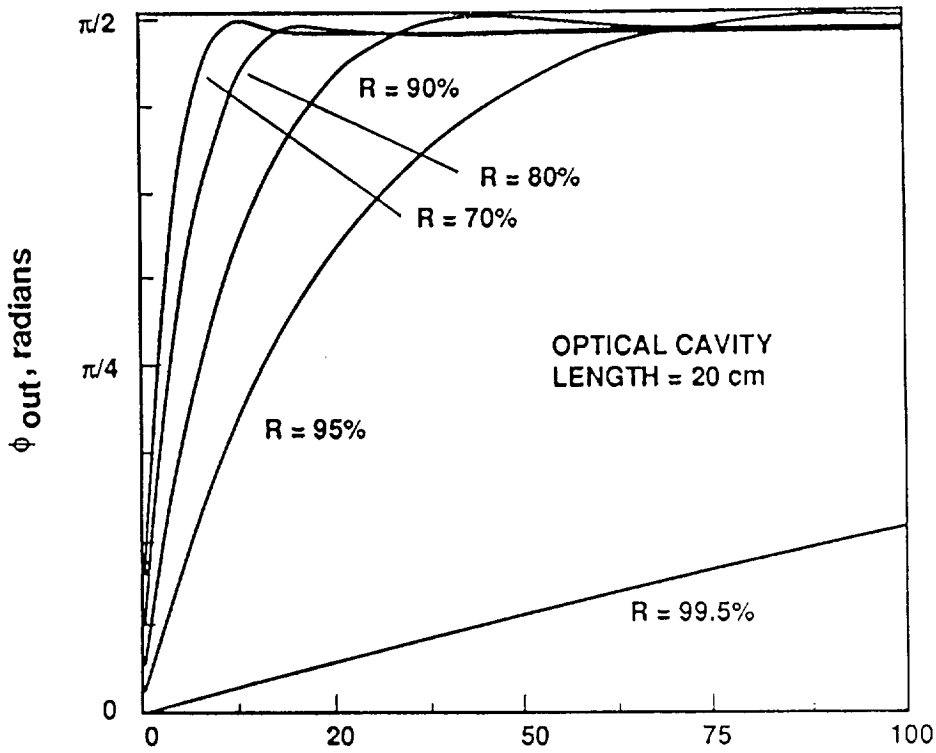
π/2
π/4
0
φ out, radians
R = 90%
R = 80%
R = 70%
R = 95%
R = 99.5%
OPTICAL CAVITY
LENGTH = 20 cm
0
20
50
75
100
TIME, nsec

FIG. 6

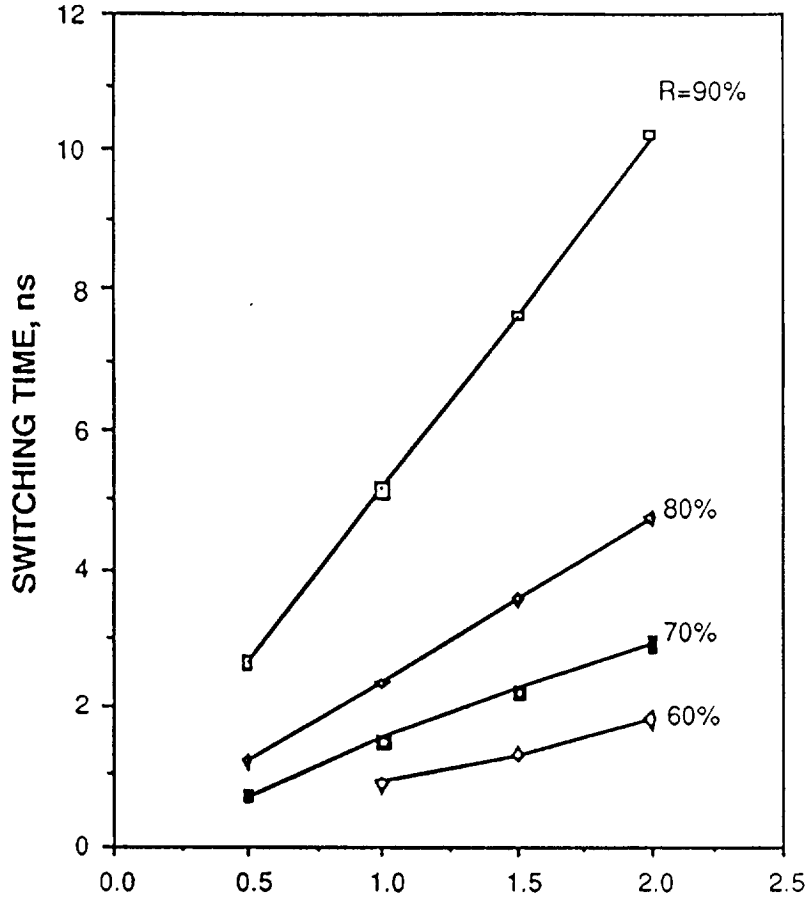
12
10
8
6
4
2
0
SWITCHING TIME, ns
R=90%
80%
70%
60%
0.0
0.5
1.0
1.5
2.0
2.5
CAVITY LENGTH, cm

FIG. 7

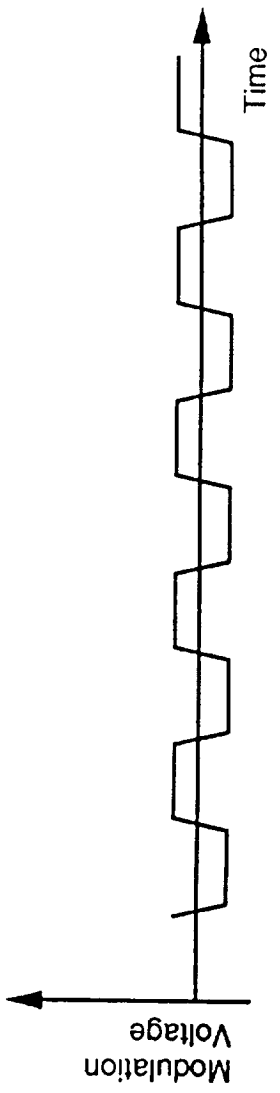
Time
Modulation
Voltage

FIG. 8(a)

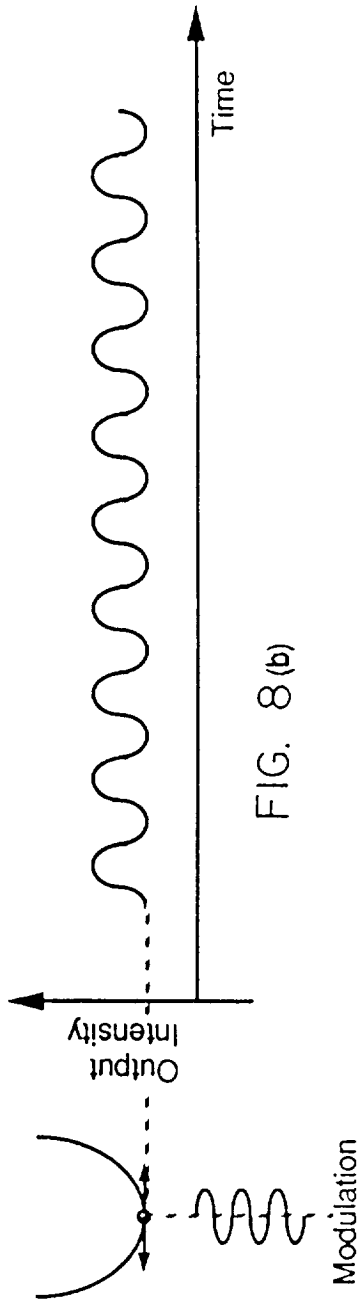
Time
Output
Intensity
Modulation

FIG. 8(b)

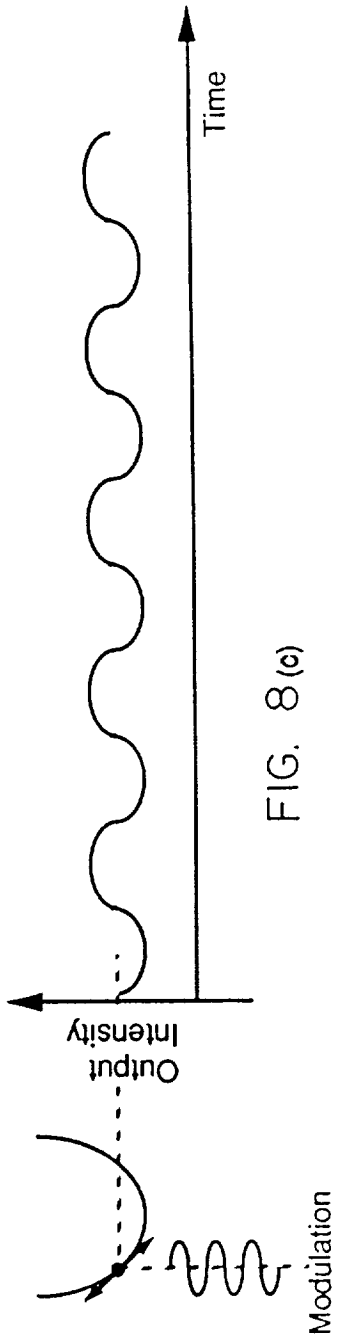
Time
Output Intensity
Modulation

FIG. 8(c)

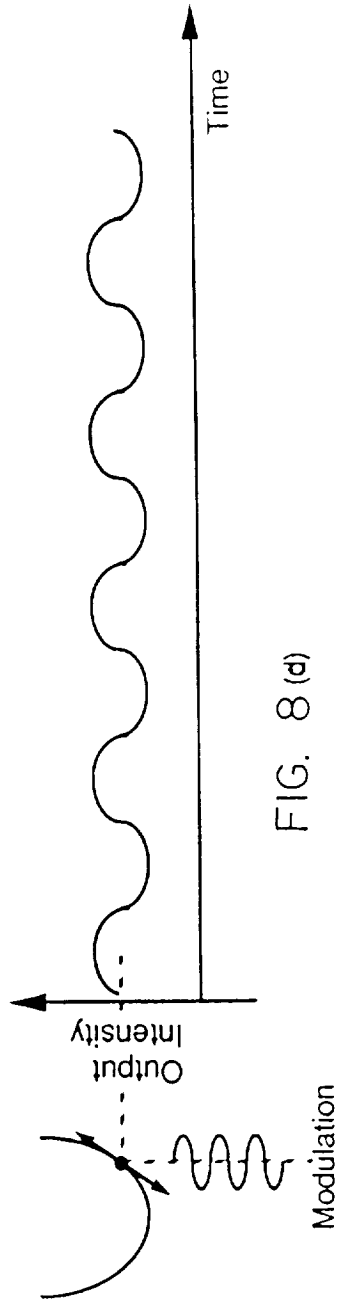
Time
Output Intensity
Modulation

FIG. 8(d)

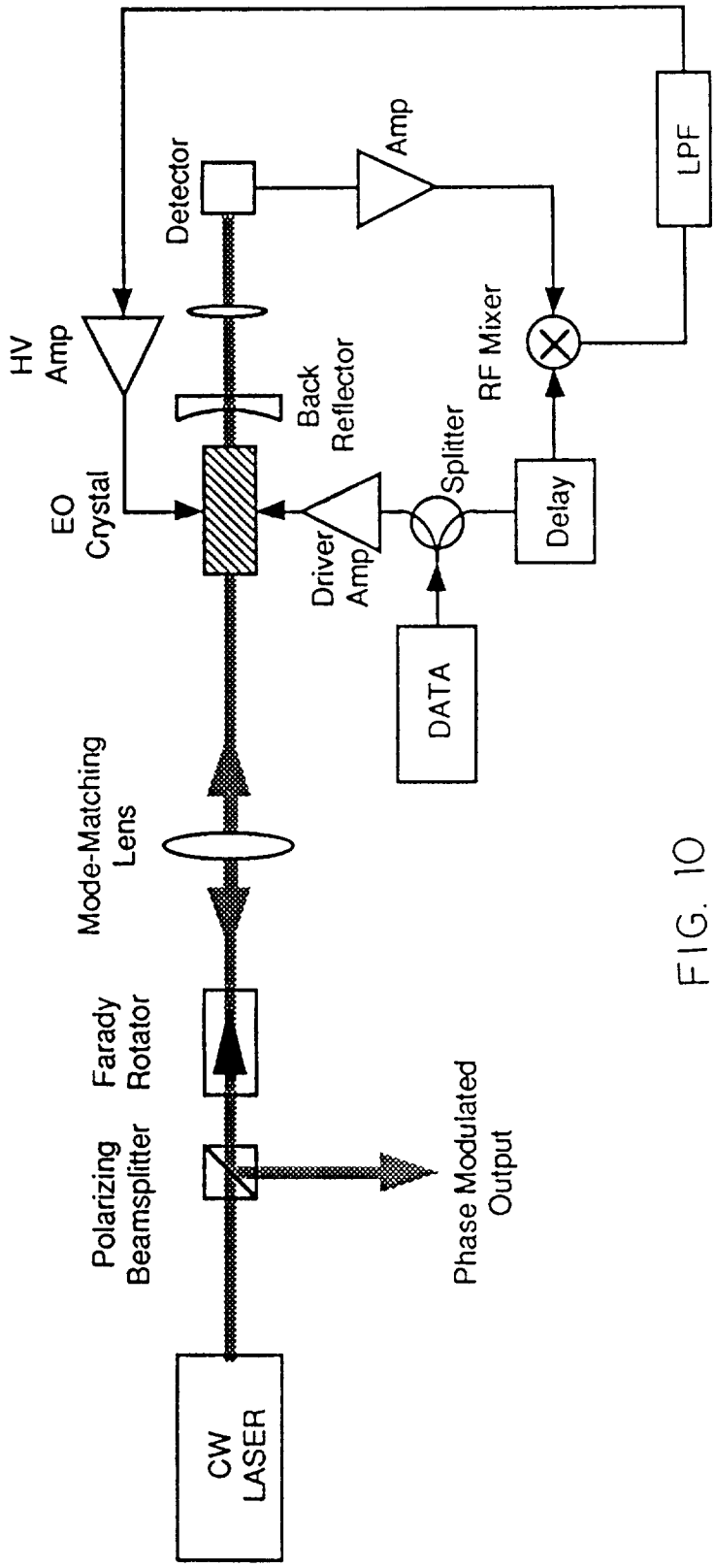
CW LASER
Polarizing Beamsplitter
Farady Rotator
Mode-Matching Lens
Phase Modulated Output
DATA
Driver Amp
EO Crystal
HV Amp
Back Reflector
Detector
Amp
Splitter
Delay
RF Mixer
LPF

FIG. 10

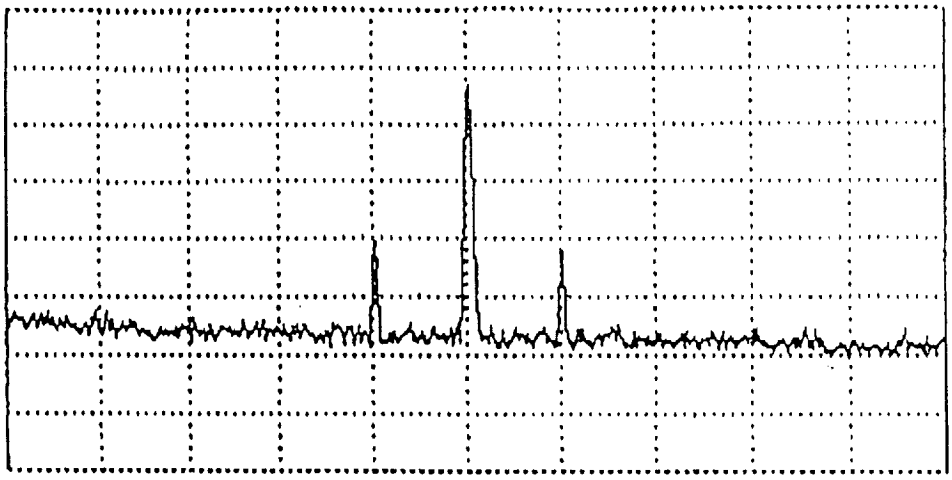

FIG. 11(a)

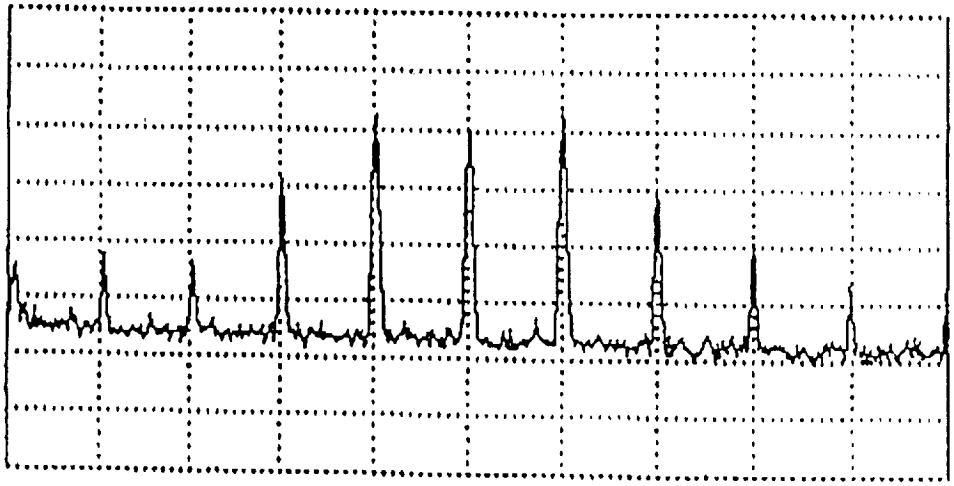

FIG. 11(b)

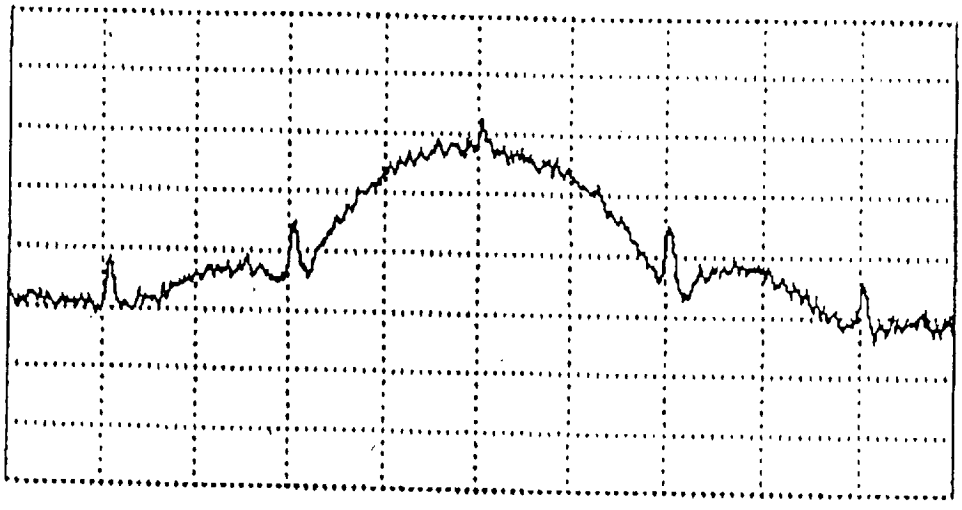

FIG. 11(c)